

Cosmological constraints from HII starburst galaxy apparent magnitude and other cosmological measurements

Shulei Cao,^{1*} Joseph Ryan,^{1†} Bharat Ratra^{1‡}

¹*Department of Physics, Kansas State University, 116 Cardwell Hall, Manhattan, KS 66502, USA*

Accepted XXX. Received YYY; in original form ZZZ

ABSTRACT

We use HII starburst galaxy apparent magnitude measurements to constrain cosmological parameters in six cosmological models. A joint analysis of HII galaxy, quasar angular size, baryon acoustic oscillations peak length scale, and Hubble parameter measurements result in relatively model-independent and restrictive estimates of the current values of the non-relativistic matter density parameter Ω_{m_0} and the Hubble constant H_0 . These estimates favor a 2.0σ to 3.4σ (depending on cosmological model) lower H_0 than what is measured from the local expansion rate. The combined data are consistent with dark energy being a cosmological constant and with flat spatial hypersurfaces, but do not strongly rule out mild dark energy dynamics or slightly non-flat spatial geometries.

Key words: cosmological parameters – dark energy – cosmology: observations

1 INTRODUCTION

The accelerated expansion of the current universe is now well-established observationally and is usually credited to a dark energy whose origins remain murky (see e.g. Ratra & Vogeley 2008; Martin 2012; Coley & Ellis 2020). The standard Λ CDM model of cosmology (Peebles 1984) describes a universe with flat spatial hypersurfaces predominantly filled with dark energy in the form of a cosmological constant Λ and cold dark matter (CDM) together comprising $\sim 95\%$ of the total energy budget. While spatially-flat Λ CDM is mostly consistent with cosmological observations (see e.g. Alam et al. 2017; Farooq et al. 2017; Scolnic et al. 2018; Planck Collaboration 2018), there are indications of some (mild) discrepancies between standard Λ CDM model predictions and cosmological measurements. In addition, the quality and quantity of cosmological data continue to grow, making it possible to consider and constrain additional cosmological parameters beyond those that characterize the standard Λ CDM model.

Given the uncertainty surrounding the origin of the cosmological constant, many workers have investigated the possibility that the cosmological “constant” is not really constant, but rather evolves in time, either by positing an equation of state parameter $w \neq -1$ (thereby introducing a redshift dependence into the dark energy density) or by replacing the constant Λ in the Einstein-Hilbert action with a dynamical scalar field ϕ (Peebles & Ratra 1988; Ratra & Peebles 1988). Non-flat spatial geometry also introduces a time-dependent source term in the Friedmann equations. In this paper we

study the standard spatially-flat Λ CDM model as well as dynamical dark energy and spatially non-flat extensions of this model.

One major goal of this paper is to use measurements of the redshift, apparent luminosity, and gas velocity dispersion of HII starburst galaxies to constrain cosmological parameters.¹ An HII starburst galaxy (hereinafter “HIIG”) is one that contains a large HII region, an emission nebula sourced by the UV radiation from an O- or B-type star. There is a correlation between the measured luminosity (L) and the inferred velocity dispersion (σ) of the ionized gases within these HIIG, referred to as the L - σ relation (see Sec. 2) which has been shown to be a useful cosmological tracer (see Melnick et al. 2000; Siegel et al. 2005; Plionis et al. 2011; Chávez et al. 2012, 2014, 2016; Terlevich et al. 2015; González-Morán et al. 2019, and references therein). This relation has been used to constrain the Hubble constant H_0 (Chávez et al. 2012; Fernández Arenas et al. 2018), and it can also be used to put constraints on the dark energy equation of state parameter w (Terlevich et al. 2015; Chávez et al. 2016; González-Morán et al. 2019).

HIIG data reach to redshift $z \sim 2.4$, a little beyond that of the highest redshift baryon acoustic oscillation (BAO) data which reach to $z \sim 2.3$. HIIG data are among a handful of cosmological observations that probe the largely unexplored part of redshift space from $z \sim 2$ to $z \sim 1100$. Other data that probe this region include quasar angular size measurements that reach to $z \sim 2.7$ (Gurvits et al. 1999; Chen & Ratra 2003; Cao et al. 2017; Ryan et al. 2019, and references therein), quasar flux measurements that reach to $z \sim 5$

¹ For early attempts see Siegel et al. (2005), Plionis et al. (2009, 2010, 2011) and Mania & Ratra (2012). For more recent discussions see Chávez et al. (2016), Wei et al. (2016), Yennapureddy & Melia (2017), Zheng et al. (2019), Ruan et al. (2019), González-Morán et al. (2019), Wan et al. (2019), and Wu et al. (2020).

* E-mail: shulei@phys.ksu.edu

† E-mail: jwryan@phys.ksu.edu

‡ E-mail: ratra@phys.ksu.edu

(Risaliti & Lusso 2015, 2019; Yang et al. 2019; Khadka & Ratra 2020a,b; Zheng et al. 2020, and references therein), and gamma ray burst data that reach to $z \sim 8$ (Lamb & Reichart 2000; Samushia & Ratra 2010; Demianski et al. 2019, and references therein). In this paper we also use quasar angular size measurements (hereinafter ‘‘QSO’’) to constrain cosmological model parameters.

While HIIG and QSO data probe the largely unexplored $z \sim 2.3$ – 2.7 part of the universe, current HIIG and QSO measurements provide relatively weaker constraints on cosmological parameters than those provided by more widely used measurements, such as BAO peak length scale observations or Hubble parameter (hereinafter ‘‘ $H(z)$ ’’) observations (with these latter data being at lower redshift but of better quality than HIIG or QSO data). However, we find that the HIIG and QSO constraints are consistent with those that follow from BAO and $H(z)$ data, and so we use all four sets of data together to constrain cosmological parameters. We find that the HIIG and QSO data tighten parameter constraints relative to the $H(z)$ + BAO only case.

Using six different cosmological models to constrain cosmological parameters allows us to determine which of our results are less model-dependent. In all models, the HIIG data favor those parts of cosmological parameter space for which the current cosmological expansion is accelerating.² The joint analysis of the HIIG, QSO, BAO and $H(z)$ data results in relatively model-independent and fairly tight determination of the Hubble constant H_0 and the current non-relativistic matter density parameter Ω_{m_0} .³ Depending on the model, Ω_{m_0} ranges from a low of $0.309^{+0.015}_{-0.014}$ to a high of 0.319 ± 0.013 , being consistent with most other estimates of this parameter (unless indicated otherwise, uncertainties given in this paper are $\pm 1\sigma$). The best-fit values of H_0 , ranging from $68.18^{+0.97}_{-0.75}$ $\text{km s}^{-1} \text{Mpc}^{-1}$ to 69.90 ± 1.48 $\text{km s}^{-1} \text{Mpc}^{-1}$, are, from the quadrature sum of the error bars, 2.01σ to 3.40σ lower than the local $H_0 = 74.03 \pm 1.42$ $\text{km s}^{-1} \text{Mpc}^{-1}$ measurement of Riess et al. (2019) and only 0.06σ to 0.60σ higher than the median statistics $H_0 = 68 \pm 2.8$ $\text{km s}^{-1} \text{Mpc}^{-1}$ estimate of Chen & Ratra (2011a). These combined measurements are consistent with the spatially-flat Λ CDM model, but also do not strongly disallow some mild dark energy dynamics, as well as a little non-zero spatial curvature density.

This paper is organized as follows. In Sec. 2 we introduce the data we use. Section 3 describes the models we analyze, with a description of our analysis method in Sec. 4. Our results are in Sec. 5, and we provide our conclusions in Sec. 6.

² This result could weaken, however, as the HIIG data constraint contours could broaden when HIIG data systematic uncertainties are taken into account. We do not incorporate any HIIG systematic uncertainties into our analysis; see below.

³ The BAO and $H(z)$ data play a more significant role than do the HIIG and QSO data in setting these and other limits, but the HIIG and QSO data tighten the BAO + $H(z)$ constraints. We note, however, that the $H(z)$ and QSO data, by themselves, give lower central values of H_0 but with larger error bars. Also, because we calibrate the distance scale of the BAO measurements listed in Table 1 via the sound horizon scale at the drag epoch (r_s , about which see below), a quantity that depends on early-Universe physics, we would expect these measurements to push the best-fit values H_0 lower when they are combined with late-Universe measurements like HIIG (whose distance scale is not set by the physics of the early Universe).

Table 1. BAO data.

z	Measurement ^d	Value	Ref.
0.38	$D_M(r_{s,\text{fid}}/r_s)$	1512.39	Alam et al. (2017) ^b
0.38	$H(z)(r_s/r_{s,\text{fid}})$	81.2087	Alam et al. (2017) ^b
0.51	$D_M(r_{s,\text{fid}}/r_s)$	1975.22	Alam et al. (2017) ^b
0.51	$H(z)(r_s/r_{s,\text{fid}})$	90.9029	Alam et al. (2017) ^b
0.61	$D_M(r_{s,\text{fid}}/r_s)$	2306.68	Alam et al. (2017) ^b
0.61	$H(z)(r_s/r_{s,\text{fid}})$	98.9647	Alam et al. (2017) ^b
0.122	$D_V(r_{s,\text{fid}}/r_s)$	539 ± 17	Carter et al. (2018)
0.81	D_A/r_s	10.75 ± 0.43	DES Collaboration (2019b)
1.52	$D_V(r_{s,\text{fid}}/r_s)$	3843 ± 147	Ata et al. (2018)
2.34	D_H/r_s	8.86	de Sainte Agathe et al. (2019) ^c
2.34	D_M/r_s	37.41	de Sainte Agathe et al. (2019) ^c

^a $D_M(r_{s,\text{fid}}/r_s)$, $D_V(r_{s,\text{fid}}/r_s)$, r_s , and $r_{s,\text{fid}}$ have units of Mpc, while $H(z)(r_s/r_{s,\text{fid}})$ has units of $\text{km s}^{-1} \text{Mpc}^{-1}$, and D_A/r_s is dimensionless.

^b The six measurements from Alam et al. (2017) are correlated; see eq. (20) of Ryan et al. (2019) for their correlation matrix.

^c The two measurements from de Sainte Agathe et al. (2019) are correlated; see eq. (27) below for their correlation matrix.

2 DATA

We use a combination of $H(z)$, BAO, QSO, and HIIG data to obtain constraints on our cosmological models. The $H(z)$ data, spanning the redshift range $0.070 \leq z \leq 1.965$, are identical to the $H(z)$ data used in Ryan et al. (2018, 2019) and compiled in Table 2 of Ryan et al. (2018); see that paper for description. The QSO data compiled by Cao et al. (2017) (listed in Table 1 of that paper) and spanning the redshift range $0.462 \leq z \leq 2.73$, are identical to that used in Ryan et al. (2019); see these papers for descriptions. Our BAO data (see Table 1) have been updated relative to Ryan et al. (2019) and span the redshift range $0.38 \leq z \leq 2.34$. Our HIIG data are new, comprising 107 low redshift ($0.0088 \leq z \leq 0.16417$) HIIG measurements, used in Chávez et al. (2014), and 46 high redshift ($0.636427 \leq z \leq 2.42935$) HIIG measurements, used in González-Morán et al. (2019).⁴ These extinction-corrected measurements (see below for a discussion of extinction correction) were very kindly provided to us by Ana Luisa González-Morán (private communications, 2019 and 2020).

In order to use BAO measurements to constrain cosmological model parameters, knowledge of the sound horizon scale at the drag epoch (r_s) is required. We compute this scale more accurately than in Ryan et al. (2019) by using the approximate formula (Aubourg et al. 2015)

$$r_s = \frac{55.154 \exp[-72.3(\Omega_{\nu_0} h^2 + 0.0006)^2]}{(\Omega_{\text{b}_0} h^2)^{0.12807} (\Omega_{\text{cb}_0} h^2)^{0.25351}}. \quad (1)$$

Here $\Omega_{\text{cb}_0} = \Omega_{\text{c}_0} + \Omega_{\text{b}_0} = \Omega_{\text{m}_0} - \Omega_{\nu_0}$ with Ω_{cb_0} , Ω_{c_0} , Ω_{b_0} , and $\Omega_{\nu_0} = 0.0014$ (following Carter et al. 2018) being the current values of the CDM + baryonic matter, CDM, baryonic matter, and neutrino energy density parameters, respectively, and the Hubble constant $H_0 = 100 h \text{ km s}^{-1} \text{Mpc}^{-1}$. Here and in what follows, a subscript of ‘0’ on a given quantity denotes the current value of that quantity. Additionally, $\Omega_{\text{b}_0} h^2$ is slightly model-dependent; the values of this parameter that we use in this paper are the same as those originally computed in Park & Ratra (2018, 2019a,c) and listed in Table 2 of Ryan et al. (2019).

As mentioned in Sec. 1, HIIG can be used as cosmological

⁴ 15 from González-Morán et al. (2019), 25 from Erb et al. (2006), Masters et al. (2014), and Maseda et al. (2014), and 6 from Terlevich et al. (2015).

probes because they exhibit a tight correlation between the observed luminosity (L) of their Balmer emission lines and the velocity dispersion (σ) of their ionized gas (as measured from the widths of the emission lines). That correlation can be expressed in the form

$$\log L = \beta \log \sigma + \gamma, \quad (2)$$

where γ and β are the intercept and slope, respectively, and $\log = \log_{10}$ here and in what follows. In order to determine the values of β and γ , it is necessary to establish the extent to which light from an HIIG is extinguished as it propagates through space. A correction must be made to the observed flux so as to account for the effect of this extinction. As mentioned above, the data we received from Ana Luisa González-Morán have been corrected for extinction. In González-Morán et al. (2019), the authors used the Gordon et al. (2003) extinction law, and in so doing found

$$\beta = 5.022 \pm 0.058, \quad (3)$$

and

$$\gamma = 33.268 \pm 0.083, \quad (4)$$

respectively. These are the values of β and γ that we use in the L - σ relation, eq. (2).

Once the luminosity of an HIIG has been established through eq. (2), this luminosity can be used, in conjunction with a measurement of the flux (f) emitted by the HIIG, to determine the distance modulus of the HIIG via

$$\mu_{\text{obs}} = 2.5 \log L - 2.5 \log f - 100.2 \quad (5)$$

(see e.g. Terlevich et al. 2015, González-Morán et al. 2019, and references therein).⁵ This quantity can then be compared to the value of the distance modulus predicted within a given cosmological model

$$\mu_{\text{th}}(\mathbf{p}, z) = 5 \log D_L(\mathbf{p}, z) + 25, \quad (6)$$

where the luminosity distance $D_L(\mathbf{p}, z)$ is related to the transverse comoving distance $D_M(\mathbf{p}, z)$ and the angular size distance $D_A(\mathbf{p}, z)$ through $D_L(\mathbf{p}, z) = (1+z)D_M(\mathbf{p}, z) = (1+z)^2 D_A(\mathbf{p}, z)$. These are functions of the redshift z and the parameters \mathbf{p} of the model in question, and

$$D_M(\mathbf{p}, z) = \begin{cases} D_C(\mathbf{p}, z) & \text{if } \Omega_{k_0} = 0, \\ \frac{c}{H_0 \sqrt{|\Omega_{k_0}|}} \sinh \left[\sqrt{|\Omega_{k_0}|} H_0 D_C(\mathbf{p}, z) / c \right] & \text{if } \Omega_{k_0} > 0, \\ \frac{c}{H_0 \sqrt{|\Omega_{k_0}|}} \sin \left[\sqrt{|\Omega_{k_0}|} H_0 D_C(\mathbf{p}, z) / c \right] & \text{if } \Omega_{k_0} < 0. \end{cases} \quad (7)$$

In the preceding equation,

$$D_C(\mathbf{p}, z) \equiv c \int_0^z \frac{dz'}{H(\mathbf{p}, z')}, \quad (8)$$

Ω_{k_0} is the current value of the spatial curvature energy density parameter, and c is the speed of light (Hogg 1999).

As the precision of cosmological observations has grown over the last few years, a tension between measurements of the Hubble constant made with early-Universe probes and measurements made with late-Universe probes has revealed itself (for a review, see Riess 2019). Whether a given cosmological observation supports a lower value of H_0 (i.e. one that is closer to the early-Universe *Planck* measurement) or a higher value of H_0 (i.e. one that is closer to

the late-Universe value measured by Riess et al. 2019) may depend on whether the distance scale associated with this observation has been set by early- or late-Universe physics. It is therefore important to know what distance scale cosmological observations have been calibrated to, so that the extent to which measurements of H_0 are pushed higher or lower by these different distance calibrations can be clearly identified.

The H_0 values we measure from the combined $H(z)$, BAO, QSO, and HIIG data are based on a combination of both early- and late-Universe distance calibrations. As mentioned above, the distance scale of our BAO measurements is set by the size of the sound horizon at the drag epoch r_s . The sound horizon, in turn, depends on $\Omega_{b_0} h^2$, which was computed by Park & Ratra (2018, 2019a,c) using early-Universe data. Our HIIG measurements, on the other hand, have been calibrated using cosmological model independent distance ladder measurements of the distances to nearby giant HII regions (see González-Morán et al. 2019 and references therein), so these data qualify as late-Universe probes. The distance scale of our QSO measurements is set by the intrinsic linear size (l_m) of the QSOs themselves, which is a late-Universe measurement (see Cao et al. 2017). Finally, our $H(z)$ data depend on late-Universe astrophysics through the modeling of the star formation histories of the galaxies whose ages are measured to obtain the Hubble parameter (although the differences between different models are not thought to have a significant effect on measurements of $H(z)$ from these galaxies; see Moresco et al. 2018, 2020).

3 COSMOLOGICAL MODELS

The redshift z is related to the scale factor a as $1+z \equiv a_0/a$ and the Hubble parameter is $H \equiv \dot{a}/a$, where the overdot denotes the time derivative. In this paper we consider three pairs of flat and non-flat cosmological models.⁶ The data we use are at $z \leq 2.73$ and in what follows we ignore the insignificant contribution that radiation makes to the late-time cosmological energy budget.

In the Λ CDM model, the Hubble parameter is

$$H(z) = H_0 \sqrt{\Omega_{m_0}(1+z)^3 + \Omega_{k_0}(1+z)^2 + \Omega_{\Lambda}}, \quad (9)$$

where Ω_{Λ} is the (constant) dark energy density parameter. In the flat Λ CDM model the parameters to be constrained are conventionally chosen to be H_0 and Ω_{m_0} . In this model $\Omega_{k_0} = 0$, which implies $\Omega_{\Lambda} = 1 - \Omega_{m_0}$. In the non-flat Λ CDM model the parameters to be constrained are H_0 , Ω_{m_0} , and Ω_{Λ} , and the curvature energy density parameter is a derived quantity, being related to the non-relativistic matter and dark energy density parameters through $\Omega_{k_0} = 1 - \Omega_{m_0} - \Omega_{\Lambda}$.

In the XCDM parametrization, dark energy is modeled as an ideal, spatially homogeneous X-fluid with equation of state $w_X = p_X/\rho_X$, where p_X and ρ_X are the X-fluid's pressure and energy

⁵ For each HIIG in our sample we have the measured values and uncertainties of $\log f$, $\log \sigma$, and z .

⁶ Observational constraints on non-flat models are discussed in Farooq et al. (2015), Chen et al. (2016), Yu & Wang (2016), Rana et al. (2017), Ooba et al. (2018a,b,c), Yu et al. (2018), Park & Ratra (2018, 2019a,b,c, 2020), Wei (2018), DES Collaboration (2019a), Ruan et al. (2019), Coley (2019), Jesus et al. (2019), Handley (2019), Wang et al. (2019), Zhai et al. (2019), Li et al. (2020), Geng et al. (2020), Kumar et al. (2020), Efstathiou & Gratton (2020), Di Valentino et al. (2020), Gao et al. (2020), and references therein.

density, respectively.⁷ In the XCDM parametrization, the Hubble parameter is

$$H(z) = H_0 \sqrt{\Omega_{m_0}(1+z)^3 + \Omega_{k_0}(1+z)^2 + \Omega_{X_0}(1+z)^{3(1+w_X)}}, \quad (10)$$

where Ω_{X_0} is the present value of the X-fluid energy density parameter. From this equation, it can be seen that when $w_X = -1$ XCDM reduces to Λ CDM. In the non-flat case the model parameters to be constrained are H_0 , Ω_{m_0} , Ω_{k_0} , and w_X , with $\Omega_{X_0} = 1 - \Omega_{m_0} - \Omega_{k_0}$ as a derived parameter (we do not report constraints on its value in this paper). In the spatially-flat case the parameters to be constrained are H_0 , Ω_{m_0} , and w_X , with $\Omega_{X_0} = 1 - \Omega_{m_0}$.

In the flat and non-flat ϕ CDM models, dark energy is modeled as a dynamical scalar field ϕ , with a potential energy density given by

$$V(\phi) = \frac{1}{2} \kappa m_p^2 \phi^{-\alpha}, \quad (11)$$

where m_p is the Planck mass, α is a non-negative scalar, and

$$\kappa = \frac{8}{3m_p^2} \left(\frac{\alpha+4}{\alpha+2} \right) \left[\frac{2}{3} \alpha (\alpha+2) \right]^{\alpha/2} \quad (12)$$

(Peebles & Ratra 1988; Ratra & Peebles 1988; Pavlov et al. 2013).⁸ Note that when $\alpha = 0$ the ϕ CDM model reduces to the Λ CDM model. In the spatially homogeneous approximation, valid for the cosmological tests we consider in this paper, the dynamics of the scalar field is governed by two coupled non-linear ordinary differential equations, the first being the scalar field equation of motion

$$\ddot{\phi} + 3 \left(\frac{\dot{a}}{a} \right) \dot{\phi} - \frac{1}{2} \alpha \kappa m_p^2 \phi^{-\alpha-1} = 0, \quad (13)$$

and the second being the Friedman equation

$$\left(\frac{\dot{a}}{a} \right)^2 = \frac{8\pi}{3m_p^2} (\rho_m + \rho_\phi) - \frac{k}{a^2}. \quad (14)$$

In eq. (14), $-k/a^2$ is the spatial curvature term (with $k = 0, -1, +1$ corresponding to $\Omega_{k_0} = 0, > 0, < 0$, respectively), and ρ_m and ρ_ϕ are the non-relativistic matter and scalar field energy densities, respectively, where

$$\rho_\phi = \frac{m_p^2}{32\pi} \left(\dot{\phi}^2 + \kappa m_p^2 \phi^{-\alpha} \right). \quad (15)$$

It follows that the Hubble parameter in ϕ CDM is

$$H(z) = H_0 \sqrt{\Omega_{m_0}(1+z)^3 + \Omega_{k_0}(1+z)^2 + \Omega_\phi(z, \alpha)}, \quad (16)$$

⁷ It should be noted, however, that the XCDM parametrization cannot sensibly describe the evolution of spatial inhomogeneities, and is therefore, unlike the Λ CDM and ϕ CDM models, physically incomplete. It is possible to extend this parametrization by allowing for an additional free parameter $c_{s,X}^2 = dp_X/d\rho_X$ and requiring that $c_{s,X}^2 > 0$.

⁸ Observational constraints on the ϕ CDM model are discussed in Chen & Ratra (2004), Samushia et al. (2007), Yashar et al. (2009), Samushia et al. (2010), Chen & Ratra (2011b), Campanelli et al. (2012), Farooq & Ratra (2013), Farooq et al. (2013), Avsajanishvili et al. (2015), Solà et al. (2017), Zhai et al. (2017), Sangwan et al. (2018), Solà Peracaula et al. (2018, 2019), Ooba et al. (2019), Singh et al. (2019), and references therein.

where the scalar field energy density parameter

$$\Omega_\phi(z, \alpha) = \frac{1}{12H_0^2} \left(\dot{\phi}^2 + \kappa m_p^2 \phi^{-\alpha} \right), \quad (17)$$

as can be determined from eqs. (13) and (14). For non-flat ϕ CDM the parameters to be constrained are α , H_0 , Ω_{m_0} , and Ω_{k_0} and for flat ϕ CDM the parameters to be constrained are α , H_0 , and Ω_{m_0} .

4 DATA ANALYSIS METHODOLOGY

We perform a Markov chain Monte Carlo (MCMC) analysis with the Python module emcee (Foreman-Mackey et al. 2013) and maximize the likelihood function, \mathcal{L} , to determine the best-fit values of the parameters \mathbf{p} of the models. We use flat priors for all parameters \mathbf{p} . For all models, the priors on Ω_{m_0} and h are non-zero over the ranges $0.1 \leq \Omega_{m_0} \leq 0.7$ and $0.50 \leq h \leq 0.85$. In the non-flat Λ CDM model the Ω_Λ prior is non-zero over $0.2 \leq \Omega_\Lambda \leq 1$. In the flat and non-flat XCDM parametrizations the prior range on w_X is $-2 \leq w_X \leq 0$, and the prior range on Ω_{k_0} in the non-flat XCDM parametrization is $-0.7 \leq \Omega_{k_0} \leq 0.7$. In the flat and non-flat ϕ CDM models the prior range on α is $0.01 \leq \alpha \leq 3$ and $0.01 \leq \alpha \leq 5$, respectively, and the prior range on Ω_{k_0} is also $-0.7 \leq \Omega_{k_0} \leq 0.7$.

For HIIG, the likelihood function is

$$\mathcal{L}_{\text{HIIG}} = e^{-\chi_{\text{HIIG}}^2/2}, \quad (18)$$

where

$$\chi_{\text{HIIG}}^2(\mathbf{p}) = \sum_{i=1}^{153} \frac{[\mu_{\text{th}}(\mathbf{p}, z_i) - \mu_{\text{obs}}(z_i)]^2}{\epsilon_i^2}, \quad (19)$$

and ϵ_i is the uncertainty of the i_{th} measurement. Following González-Morán et al. (2019), ϵ has the form

$$\epsilon = \sqrt{\epsilon_{\text{stat}}^2 + \epsilon_{\text{sys}}^2}, \quad (20)$$

where the statistical uncertainties are

$$\epsilon_{\text{stat}}^2 = 6.25 \left[\epsilon_{\log f}^2 + \beta^2 \epsilon_{\log \sigma}^2 + \epsilon_{\beta}^2 (\log \sigma)^2 + \epsilon_{\gamma}^2 \right] + \left(\frac{\partial \mu_{\text{th}}}{\partial z} \right)^2 \epsilon_z^2. \quad (21)$$

Following González-Morán et al. (2019) we do not account for systematic uncertainties in our analysis, so the uncertainty on the HIIG measurements consists entirely of the statistical uncertainty (so that $\epsilon = \epsilon_{\text{stat}}$).⁹ The reader should also note here that although the theoretical statistical uncertainty depends our cosmological model parameters (through the theoretical distance modulus $\mu_{\text{th}} = \mu_{\text{th}}(\mathbf{p}, z)$), the effect of this model-dependence on the parameter constraints is negligible for the current data.¹⁰

⁹ A systematic error budget for HIIG data is available in the literature, however; see Chávez et al. (2016).

¹⁰ In contrast to our definition of χ^2 in eq. (19), González-Morán et al. (2019) defined an H_0 -independent χ^2 function in their eq. (27) and weighted this χ^2 function by $1/\epsilon_{\text{stat}}^2$ (where ϵ_{stat}^2 is given by their eq. (15)) which we do not do. This procedure is discussed in the literature (Melnick et al. 2017; Fernández Arenas et al. 2018), and when we use it we find that it leads to a reduced χ^2 identical to that given in González-Morán et al. (2019) (being less than 2 but greater than 1) without having a noticeable effect on the shapes or peak locations of our posterior likelihoods (hence providing very similar best-fit values and error bars of the cosmological model parameters). As discussed below, with our χ^2 definition we find reduced χ^2 values ~ 2.75 . González-Morán et al. (2019) note that an accounting of systematic uncertainties could decrease the reduced χ^2 values towards unity.

For $H(z)$, the likelihood function is

$$\mathcal{L}_H = e^{-\chi_H^2/2}, \quad (22)$$

where

$$\chi_H^2(\mathbf{p}) = \sum_{i=1}^{31} \frac{[H_{\text{th}}(\mathbf{p}, z_i) - H_{\text{obs}}(z_i)]^2}{\epsilon_i^2}, \quad (23)$$

and ϵ_i is the uncertainty of $H_{\text{obs}}(z_i)$.

For the BAO data, the likelihood function is

$$\mathcal{L}_{\text{BAO}} = e^{-\chi_{\text{BAO}}^2/2}, \quad (24)$$

and for the uncorrelated BAO data (lines 7-9 in Table 1) the χ^2 function takes the form

$$\chi_{\text{BAO}}^2(\mathbf{p}) = \sum_{i=1}^3 \frac{[A_{\text{th}}(\mathbf{p}, z_i) - A_{\text{obs}}(z_i)]^2}{\epsilon_i^2}, \quad (25)$$

where A_{th} and A_{obs} are, respectively, the theoretical and observational quantities as listed in Table 1, and ϵ_i corresponds to the uncertainty of $A_{\text{obs}}(z_i)$. For the correlated BAO data, the χ^2 function takes the form

$$\chi_{\text{BAO}}^2(\mathbf{p}) = [A_{\text{th}}(\mathbf{p}) - A_{\text{obs}}(z_i)]^T \mathbf{C}^{-1} [A_{\text{th}}(\mathbf{p}) - A_{\text{obs}}(z_i)], \quad (26)$$

where superscripts T and -1 denote the transpose and inverse of the matrices, respectively. The covariance matrix \mathbf{C} for the BAO data, taken from Alam et al. (2017), is given in eq. (20) of Ryan et al. (2019), while for the BAO data from de Sainte Agathe et al. (2019),

$$\mathbf{C} = \begin{bmatrix} 0.0841 & -0.183396 \\ -0.183396 & 3.4596 \end{bmatrix}. \quad (27)$$

For QSO, the likelihood function is

$$\mathcal{L}_{\text{QSO}} = e^{-\chi_{\text{QSO}}^2/2}, \quad (28)$$

and the χ^2 function takes the form

$$\chi_{\text{QSO}}^2(\mathbf{p}) = \sum_{i=1}^{120} \left[\frac{\theta_{\text{th}}(\mathbf{p}, z_i) - \theta_{\text{obs}}(z_i)}{\epsilon_i + 0.1\theta_{\text{obs}}(z_i)} \right]^2, \quad (29)$$

where $\theta_{\text{th}}(\mathbf{p}, z_i)$ and $\theta_{\text{obs}}(z_i)$ are theoretical and observed values of the angular size at redshift z_i , respectively, and ϵ_i is the uncertainty of $\theta_{\text{obs}}(z_i)$ (see Ryan et al. 2019 for more details).

For the joint analysis of these data, the total likelihood function is obtained by multiplying the individual likelihood functions (that is, eqs. (18), (22), (24), and (28)) together in various combinations. For example, for $H(z)$, BAO, and QSO data, we have

$$\mathcal{L} = \mathcal{L}_H \mathcal{L}_{\text{BAO}} \mathcal{L}_{\text{QSO}}. \quad (30)$$

We also use the Akaike Information Criterion (AIC) and Bayesian Information Criterion (BIC) to compare the goodness of fit of models with different numbers of parameters, where

$$AIC = -2 \ln \mathcal{L}_{\text{max}} + 2n \equiv \chi_{\text{min}}^2 + 2n, \quad (31)$$

and

$$BIC = -2 \ln \mathcal{L}_{\text{max}} + n \ln N \equiv \chi_{\text{min}}^2 + n \ln N. \quad (32)$$

In these two equations, \mathcal{L}_{max} refers to the maximum value of the given likelihood function, χ_{min}^2 refers to the corresponding minimum χ^2 value, n is the number of parameters of the given model, and N is the number of data points (for example for HIIG we have $N = 153$, etc.).

5 RESULTS

5.1 HIIG constraints

We present the posterior one-dimensional (1D) probability distributions and two-dimensional (2D) confidence regions of the cosmological parameters for the six flat and non-flat models in Figs. 1–6, in gray. The unmarginalized best-fit parameter values are listed in Table 2, along with the corresponding χ^2 , AIC , BIC , and degrees of freedom ν (where $\nu \equiv N - n$). The marginalized best-fit parameter values and uncertainties ($\pm 1\sigma$ error bars or 2σ limits) are given in Table 3.¹¹

From the fit to the HIIG data, we see that most of the probability lies in the part of the parameter space corresponding to currently-accelerating cosmological expansion (see the gray contours in Figs. 1–6). This means that the HIIG data favor currently-accelerating cosmological expansion,¹² in agreement with supernova Type Ia, BAO, $H(z)$, and other cosmological data.

From the HIIG data, we find that the constraints on the non-relativistic matter density parameter $\Omega_{\text{m}0}$ are consistent with other estimates, ranging between a high of $0.300^{+0.106}_{-0.083}$ (flat Λ CDM) and a low of $\Omega_{\text{m}0} = 0.210^{+0.043}_{-0.092}$ (flat ϕ CDM).

The HIIG data constraints on H_0 in Table 3 are consistent with the estimate of $H_0 = 71.0 \pm 2.8$ (stat.) ± 2.1 (sys.) $\text{km s}^{-1} \text{Mpc}^{-1}$ made by Fernández Arenas et al. (2018) based on a compilation of HIIG measurements that differs from what we have used here. The HIIG H_0 constraints listed in Table 3 are also consistent with other recent measurements of H_0 , being between 0.90σ (flat Λ CDM) and 1.56σ (non-flat ϕ CDM) lower than the recent local expansion rate measurement of $H_0 = 74.03 \pm 1.42 \text{ km s}^{-1} \text{Mpc}^{-1}$ (Riess et al. 2019),¹³ and between 0.78σ (non-flat ϕ CDM) and 1.13σ (flat Λ CDM) higher than the median statistics estimate of $H_0 = 68 \pm 2.8 \text{ km s}^{-1} \text{Mpc}^{-1}$ (Chen & Ratra 2011a),¹⁴ with our measurements ranging from a low of $H_0 = 70.60^{+1.68}_{-1.84} \text{ km s}^{-1} \text{Mpc}^{-1}$ (non-flat ϕ CDM) to a high of $H_0 = 71.85 \pm 1.96 \text{ km s}^{-1} \text{Mpc}^{-1}$ (flat Λ CDM).

As for spatial curvature, from the marginalized 1D likelihoods in Table 3, for non-flat Λ CDM, non-flat Λ XCDM, and non-flat ϕ CDM, we measure $\Omega_{\text{k}0} = 0.094^{+0.237}_{-0.363}$,¹⁵ $\Omega_{\text{k}0} = 0.011^{+0.457}_{-0.460}$, and $\Omega_{\text{k}0} = 0.291^{+0.348}_{-0.113}$, respectively. From the marginalized likelihoods, we see that non-flat Λ CDM and Λ XCDM models are consistent with all three spatial geometries, while non-flat ϕ CDM favors the open case at 2.58σ . However, this seems to be a little odd, especially

¹¹ We plot these figures by using the Python package GetDist (Lewis 2019), which we also use to compute the central values (posterior means) and uncertainties of the cosmological parameters listed in Table 3.

¹² Although a full accounting of the systematic uncertainties in the HIIG data could weaken this conclusion.

¹³ Note that other local expansion rate measurements are slightly lower with slightly larger error bars (Rigault et al. 2015; Zhang et al. 2017; Dhawan et al. 2018; Fernández Arenas et al. 2018; Freedman et al. 2019, 2020; Rameez & Sarkar 2019).

¹⁴ This is consistent with earlier median statistics estimates (Gott et al. 2001; Chen et al. 2003) and also with a number of recent H_0 measurements (Chen et al. 2017; DES Collaboration 2018; Gómez-Valent & Amendola 2018; Haridasu et al. 2018; Planck Collaboration 2018; Zhang 2018; Domínguez et al. 2019; Martinelli & Tutusaus 2019; Cuceu et al. 2019; Zeng & Yan 2019; Schöneberg et al. 2019; Lin & Ishak 2019; Zhang & Huang 2019).

¹⁵ Since $\Omega_{\text{k}0} = 1 - \Omega_{\text{m}0} - \Omega_{\Lambda}$, in the non-flat Λ CDM model analysis we replace Ω_{Λ} with $\Omega_{\text{k}0}$ in the MCMC chains of $\{H_0, \Omega_{\text{m}0}, \Omega_{\Lambda}\}$ to obtain new chains of $\{H_0, \Omega_{\text{m}0}, \Omega_{\text{k}0}\}$ and so measure $\Omega_{\text{k}0}$ central values and uncertainties. A similar procedure, based on $\Omega_{\Lambda} = 1 - \Omega_{\text{m}0}$, is used to measure Ω_{Λ} in the flat Λ CDM model.

for non-flat ϕ CDM, considering their unmarginalized best-fit Ω_{k_0} 's are all negative (see Table 2).

The fits to the HIIG data are consistent with dark energy being a cosmological constant but don't rule out dark energy dynamics. For flat (non-flat) XCDM, $w_X = -1.180^{+0.560}_{-0.330}$ ($w_X = -1.125^{+0.537}_{-0.321}$), which are both within 1σ of $w_X = -1$. For flat (non-flat) ϕ CDM, 2σ upper limits of α are $\alpha < 2.784$ ($\alpha < 4.590$), with the 1D likelihood functions, in both cases, peaking at $\alpha = 0$.

Current HIIG data do not provide very restrictive constraints on cosmological model parameters, but when used in conjunction with other cosmological data they can help tighten the constraints.

5.2 $H(z)$, BAO, and HIIG (HzBH) constraints

The HIIG constraints discussed in the previous subsection are consistent with constraints from most other cosmological data, so it is appropriate to use the HIIG data in conjunction with other data to constrain parameters. In this subsection we perform a full analysis of $H(z)$, BAO, and HIIG (HzBH) data and derive tighter constraints on cosmological parameters.

The 1D probability distributions and 2D confidence regions of the cosmological parameters for the six flat and non-flat models are shown in Figs. 1–6, in red. The best-fit results and uncertainties are listed in Tables 2 and 3.

When we fit our cosmological models to the HzBH data we find that the measured values of the matter density parameter Ω_{m_0} fall within a narrower range in comparison to the HIIG only case, being between 0.314 ± 0.015 (non-flat Λ CDM) and $0.323^{+0.014}_{-0.016}$ (flat ϕ CDM).

Similarly, the measured values of H_0 also fall within a narrower range when our models are fit to the HzBH data combination (and are in better agreement with the median statistics estimate of H_0 from Chen & Ratra 2011a than with the local measurement carried out by Riess et al. 2019; this is because the $H(z)$ and BAO data favor a lower H_0 value) being between $H_0 = 68.36^{+1.05}_{-0.86}$ km s⁻¹ Mpc⁻¹ (flat ϕ CDM) and 70.21 ± 1.33 km s⁻¹ Mpc⁻¹ (non-flat Λ CDM). We assume that the tension between early- and late-Universe measurements of H_0 is not a major issue here, because the 2D and 1D contours in Fig. 1 overlap, and so we compute a combined H_0 value (but if one is concerned about the early- vs late-Universe H_0 tension then one should not compare our combined-data H_0 's here, and in Secs. 5.3 and 5.4, directly to the measurements of Riess et al. 2019 or of Planck Collaboration 2018).

In contrast to the HIIG only cases, when fit to the HzBH data combination the non-flat models mildly favor closed spatial hypersurfaces. This is because the $H(z)$ and BAO data mildly favor closed spatial hypersurfaces; see, e.g. Park & Ratra (2019b) and Ryan et al. (2019). For non-flat Λ CDM, non-flat XCDM, and non-flat ϕ CDM, we find $\Omega_{k_0} = -0.029^{+0.049}_{-0.048}$, $\Omega_{k_0} = -0.082^{+0.135}_{-0.119}$, and $\Omega_{k_0} = -0.153^{+0.114}_{-0.079}$, respectively, with the non-flat ϕ CDM model favoring closed spatial hypersurfaces at 1.34σ .

The fit to the HzBH data combination produces weaker evidence for dark energy dynamics (in comparison to the HIIG only case) with tighter error bars on the measured values of w_X and α . For flat (non-flat) XCDM, $w_X = -1.052^{+0.092}_{-0.082}$ ($w_X = -0.958^{+0.219}_{-0.098}$), with $w_X = -1$ still being within the 1σ range. For flat (non-flat) ϕ CDM, $\alpha < 0.411$ ($\alpha = 0.538^{+0.151}_{-0.519}$), where the former is peaked at $\alpha = 0$ but for the latter, $\alpha = 0$ is just out of the 1σ range.

5.3 $H(z)$, BAO, and QSO (HzBQ) constraints

The $H(z)$, BAO, and QSO (HzBQ) data combination has previously been studied (Ryan et al. 2019). Relative to that analysis, we use an updated BAO data compilation, a more accurate formula for r_s , and the MCMC formalism (instead of the grid-based χ^2 approach); consequently the parameter constraints derived here slightly differ from those of Ryan et al. (2019).

The 1D probability distributions and 2D confidence regions of the cosmological parameters for all models are presented in Figs. 1–6, in green. The corresponding best-fit results and uncertainties are listed in Tables 2 and 3.

The measured values of Ω_{m_0} here fall within a similar range to the range quoted in the last subsection, being between $0.313^{+0.013}_{-0.015}$ (non-flat Λ CDM) and $0.324^{+0.014}_{-0.015}$ (flat ϕ CDM). This range is larger than, but still consistent with, the range of Ω_{m_0} reported in Ryan et al. (2019), where the same models are fit to the HzBQ data combination.

The H_0 measurements in this case fall within a broader range than in the HzBH case, being between $65.94^{+1.75}_{-1.73}$ km s⁻¹ Mpc⁻¹ (non-flat ϕ CDM) and 68.60 ± 0.68 km s⁻¹ Mpc⁻¹ (flat Λ CDM). In addition, they are lower than the corresponding measurements in the HzBH cases, and are in better agreement with the median statistics (Chen & Ratra 2011a) estimate of H_0 than with what is measured from the local expansion rate (Riess et al. 2019). Compared with Ryan et al. (2019), the central values are lower except for the non-flat XCDM model.

For non-flat Λ CDM, non-flat XCDM, and non-flat ϕ CDM, we measure $\Omega_{k_0} = 0.029^{+0.056}_{-0.063}$, $\Omega_{k_0} = -0.078^{+0.124}_{-0.112}$, and $\Omega_{k_0} = -0.103^{+0.111}_{-0.091}$, respectively. These results are consistent with their unmarginalized best-fits (see Table 2), where the best-fit to the non-flat Λ CDM model favors open spatial hypersurfaces, and the best-fits to the non-flat XCDM parametrization and the non-flat ϕ CDM model both favor closed spatial hypersurfaces. Note that the central values are larger than those of Ryan et al. (2019), especially for non-flat Λ CDM (positive instead of negative). In all three models the constraints are consistent with flat spatial hypersurfaces.

The fit to the HzBQ data combination provides slightly stronger evidence for dark energy dynamics than does the fit to the HzBH data combination. For flat (non-flat) XCDM, $w_X = -0.911^{+0.122}_{-0.098}$ ($w_X = -0.826^{+0.185}_{-0.088}$), with the former barely within 1σ of $w_X = -1$ and the latter almost 2σ away from $w_X = -1$. For flat (non-flat) ϕ CDM, $\alpha = 0.460^{+0.116}_{-0.440}$ ($\alpha = 0.854^{+0.379}_{-0.594}$), with the former 1.05σ and the latter 1.44σ away from the $\alpha = 0$ cosmological constant. In comparison with Ryan et al. (2019), central values of w_X are larger and smaller for flat and non-flat XCDM models, respectively, and that of α are larger for both flat and non-flat ϕ CDM models.

5.4 $H(z)$, BAO, QSO, and HIIG (HzBQH) constraints

Comparing the results of the previous two subsections, we see that when used in conjunction with $H(z)$ and BAO data, the QSO data result in tighter constraints on Ω_{m_0} , Ω_{k_0} (in non-flat XCDM), w_X (in non-flat XCDM), and H_0 (in flat Λ CDM), while the HIIG data result in tighter constraints on H_0 (except for flat Λ CDM), Ω_{Λ} , Ω_{k_0} (in non-flat Λ CDM and ϕ CDM), w_X (in flat XCDM), and α . Consequently, it is useful to derive constraints from an analysis of the combined $H(z)$, BAO, QSO, and HIIG (HzBQH) data. We present the results of such an analysis in this subsection.

In Figs. 1–6, we present the 1D probability distributions and

Table 2. Unmarginalized best-fit parameter values for all models from various combinations of data.

Model	Data set	Ω_{m_0}	Ω_Λ	Ω_{k_0}	w_X	α	H_0^a	χ^2	AIC	BIC	ν
Flat Λ CDM	HIIG	0.276	0.724	—	—	—	71.81	410.75	414.75	420.81	151
	$H(z)$ + BAO + HIIG	0.318	0.682	—	—	—	69.22	434.29	438.29	444.84	193
	$H(z)$ + BAO + QSO	0.315	0.685	—	—	—	68.61	372.88	376.88	383.06	160
	$H(z)$ + BAO + QSO + HIIG	0.315	0.685	—	—	—	69.06	786.50	790.50	798.01	313
Non-flat Λ CDM	HIIG	0.312	0.998	-0.310	—	—	72.35	410.44	416.44	425.53	150
	$H(z)$ + BAO + HIIG	0.313	0.718	-0.031	—	—	70.24	433.38	439.38	449.19	192
	$H(z)$ + BAO + QSO	0.311	0.665	0.024	—	—	68.37	372.82	378.82	388.08	159
	$H(z)$ + BAO + QSO + HIIG	0.309	0.716	-0.025	—	—	69.82	785.79	791.79	803.05	312
Flat XCDM	HIIG	0.249	—	—	-0.892	—	71.65	410.72	416.72	425.82	150
	$H(z)$ + BAO + HIIG	0.314	—	—	-1.044	—	69.94	433.99	439.99	449.81	192
	$H(z)$ + BAO + QSO	0.322	—	—	-0.890	—	66.62	371.95	377.95	387.21	159
	$H(z)$ + BAO + QSO + HIIG	0.311	—	—	-1.045	—	69.80	786.19	792.19	803.45	312
Non-flat XCDM	HIIG	0.104	—	-0.646	-0.712	—	72.61	407.69	415.69	427.81	149
	$H(z)$ + BAO + HIIG	0.322	—	-0.117	-0.878	—	66.67	432.85	440.85	453.94	191
	$H(z)$ + BAO + QSO	0.322	—	-0.112	-0.759	—	65.80	370.68	378.68	391.03	158
	$H(z)$ + BAO + QSO + HIIG	0.310	—	-0.048	-0.957	—	69.53	785.70	793.70	808.71	311
Flat ϕ CDM	HIIG	0.255	—	—	—	0.261	71.70	410.70	416.70	425.80	150
	$H(z)$ + BAO + HIIG	0.318	—	—	—	0.011	69.09	434.36	440.36	450.18	192
	$H(z)$ + BAO + QSO	0.321	—	—	—	0.281	66.82	372.05	378.05	387.31	159
	$H(z)$ + BAO + QSO + HIIG	0.315	—	—	—	0.012	68.95	786.58	792.58	803.84	312
Non-flat ϕ CDM	HIIG	0.114	—	-0.437	—	2.680	72.14	409.91	417.91	430.03	149
	$H(z)$ + BAO + HIIG	0.321	—	-0.132	—	0.412	69.69	432.75	440.75	453.84	191
	$H(z)$ + BAO + QSO	0.317	—	-0.106	—	0.778	66.27	370.83	378.83	391.18	158
	$H(z)$ + BAO + QSO + HIIG	0.310	—	-0.054	—	0.150	69.40	785.65	793.65	808.66	311

^a km s⁻¹ Mpc⁻¹.

Table 3. One-dimensional marginalized best-fit parameter values and uncertainties ($\pm 1\sigma$ error bars or 2σ limits) for all models from various combinations of data.

Model	Data set	Ω_{m_0}	Ω_Λ	Ω_{k_0}	w_X	α	H_0^a
Flat Λ CDM	HIIG	0.289 ^{+0.053} _{-0.071}	—	—	—	—	71.70 \pm 1.83
	$H(z)$ + BAO + HIIG	0.319 ^{+0.014} _{-0.013}	—	—	—	—	69.23 \pm 0.74
	$H(z)$ + BAO + QSO	0.316 ^{+0.013} _{-0.014}	—	—	—	—	68.60 \pm 0.68
	$H(z)$ + BAO + QSO + HIIG	0.315 ^{+0.013} _{-0.012}	—	—	—	—	69.06 ^{+0.63} _{-0.62}
Non-flat Λ CDM	HIIG	0.275 ^{+0.081} _{-0.078}	> 0.501 ^b	0.094 ^{+0.237} _{-0.363}	—	—	71.50 ^{+1.80} _{-1.81}
	$H(z)$ + BAO + HIIG	0.314 \pm 0.015	0.714 ^{+0.054} _{-0.049}	-0.029 ^{+0.049} _{-0.048}	—	—	70.21 \pm 1.33
	$H(z)$ + BAO + QSO	0.313 ^{+0.013} _{-0.015}	0.658 ^{+0.069} _{-0.060}	0.029 ^{+0.056} _{-0.063}	—	—	68.29 \pm 1.47
	$H(z)$ + BAO + QSO + HIIG	0.310 \pm 0.013	0.711 ^{+0.053} _{-0.048}	-0.021 ^{+0.044} _{-0.048}	—	—	69.76 ^{+1.12} _{-1.11}
Flat XCDM	HIIG	0.300 ^{+0.106} _{-0.083}	—	—	-1.180 ^{+0.560} _{-0.330}	—	71.85 \pm 1.96
	$H(z)$ + BAO + HIIG	0.315 ^{+0.016} _{-0.017}	—	—	-1.052 ^{+0.092} _{-0.082}	—	70.05 \pm 1.54
	$H(z)$ + BAO + QSO	0.322 ^{+0.015} _{-0.016}	—	—	-0.911 ^{+0.122} _{-0.098}	—	66.98 ^{+1.95} _{-2.30}
	$H(z)$ + BAO + QSO + HIIG	0.312 \pm 0.014	—	—	-1.053 ^{+0.091} _{-0.082}	—	69.90 \pm 1.48
Non-flat XCDM	HIIG	0.275 ^{+0.084} _{-0.125}	—	0.011 ^{+0.457} _{-0.460}	-1.125 ^{+0.537} _{-0.321}	—	71.71 ^{+2.07} _{-2.08}
	$H(z)$ + BAO + HIIG	0.318 \pm 0.019	—	-0.082 ^{+0.135} _{-0.119}	-0.958 ^{+0.219} _{-0.183}	—	69.83 ^{+1.50} _{-1.62}
	$H(z)$ + BAO + QSO	0.320 \pm 0.015	—	-0.078 ^{+0.124} _{-0.112}	-0.826 ^{+0.183} _{-0.088}	—	66.29 ^{+1.96} _{-2.35}
	$H(z)$ + BAO + QSO + HIIG	0.309 ^{+0.015} _{-0.014}	—	-0.025 \pm 0.092	-1.022 ^{+0.208} _{-0.104}	—	69.68 ^{+1.49} _{-1.64}
Flat ϕ CDM	HIIG	0.210 ^{+0.043} _{-0.092}	—	—	—	< 2.784	71.23 ^{+1.79} _{-1.80}
	$H(z)$ + BAO + HIIG	0.323 ^{+0.014} _{-0.016}	—	—	—	< 0.411	68.36 ^{+1.05} _{-0.86}
	$H(z)$ + BAO + QSO	0.324 ^{+0.014} _{-0.015}	—	—	—	0.460 ^{+0.116} _{-0.440}	66.03 ^{+1.79} _{-1.42}
	$H(z)$ + BAO + QSO + HIIG	0.319 \pm 0.013	—	—	—	< 0.411	68.18 ^{+0.97} _{-0.75}
Non-flat ϕ CDM	HIIG	< 0.321	—	0.291 ^{+0.348} _{-0.113}	—	< 4.590	70.60 ^{+1.68} _{-1.84}
	$H(z)$ + BAO + HIIG	0.322 ^{+0.015} _{-0.016}	—	-0.153 ^{+0.114} _{-0.079}	—	0.538 ^{+0.151} _{-0.319}	69.39 \pm 1.37
	$H(z)$ + BAO + QSO	0.319 ^{+0.013} _{-0.015}	—	-0.103 ^{+0.111} _{-0.091}	—	0.854 ^{+0.319} _{-0.594}	65.94 ^{+1.75} _{-1.73}
	$H(z)$ + BAO + QSO + HIIG	0.313 ^{+0.012} _{-0.014}	—	-0.098 ^{+0.082} _{-0.061}	—	< 0.926	68.83 \pm 1.23

^a km s⁻¹ Mpc⁻¹.

^b This is the 1σ lower limit. The 2σ lower limit is set by the prior, and is not shown here.

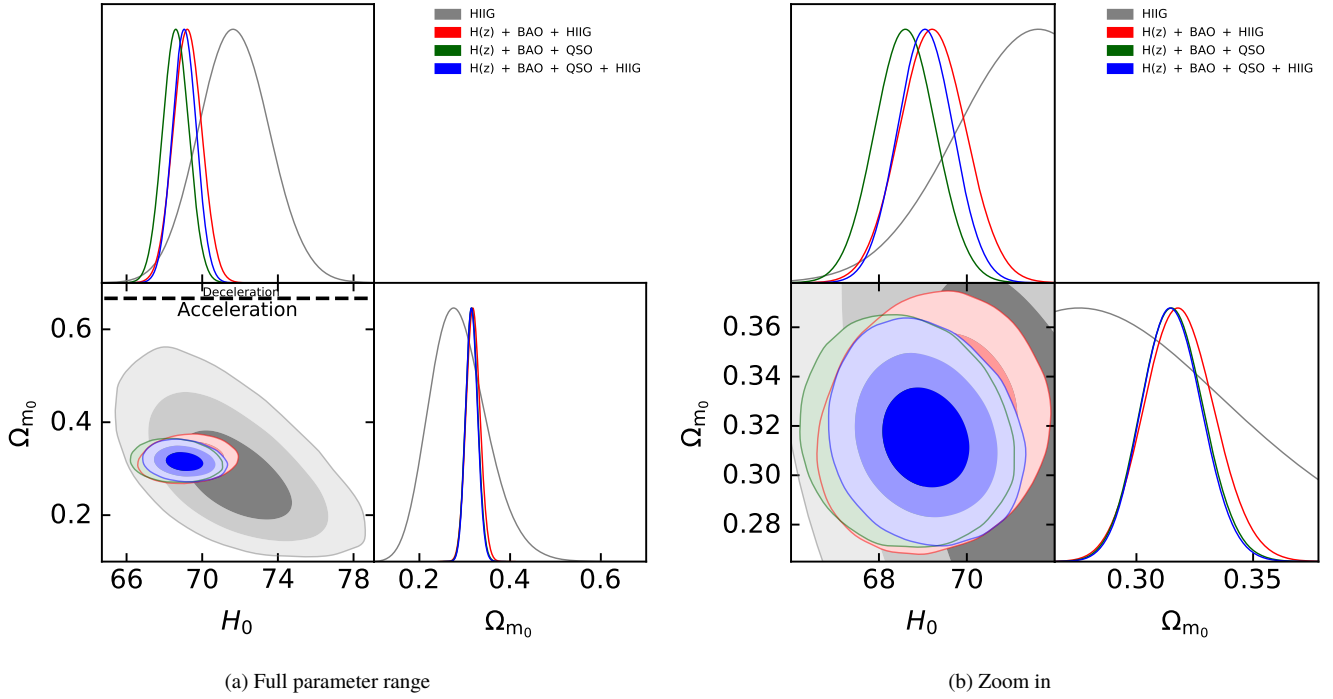


Figure 1. 1σ , 2σ , and 3σ confidence contours for flat Λ CDM, where the right panel is the comparison zoomed in. The black dotted line is the zero-acceleration line, which divides the parameter space into regions associated with currently accelerated (below) and currently decelerated (above) cosmological expansion.

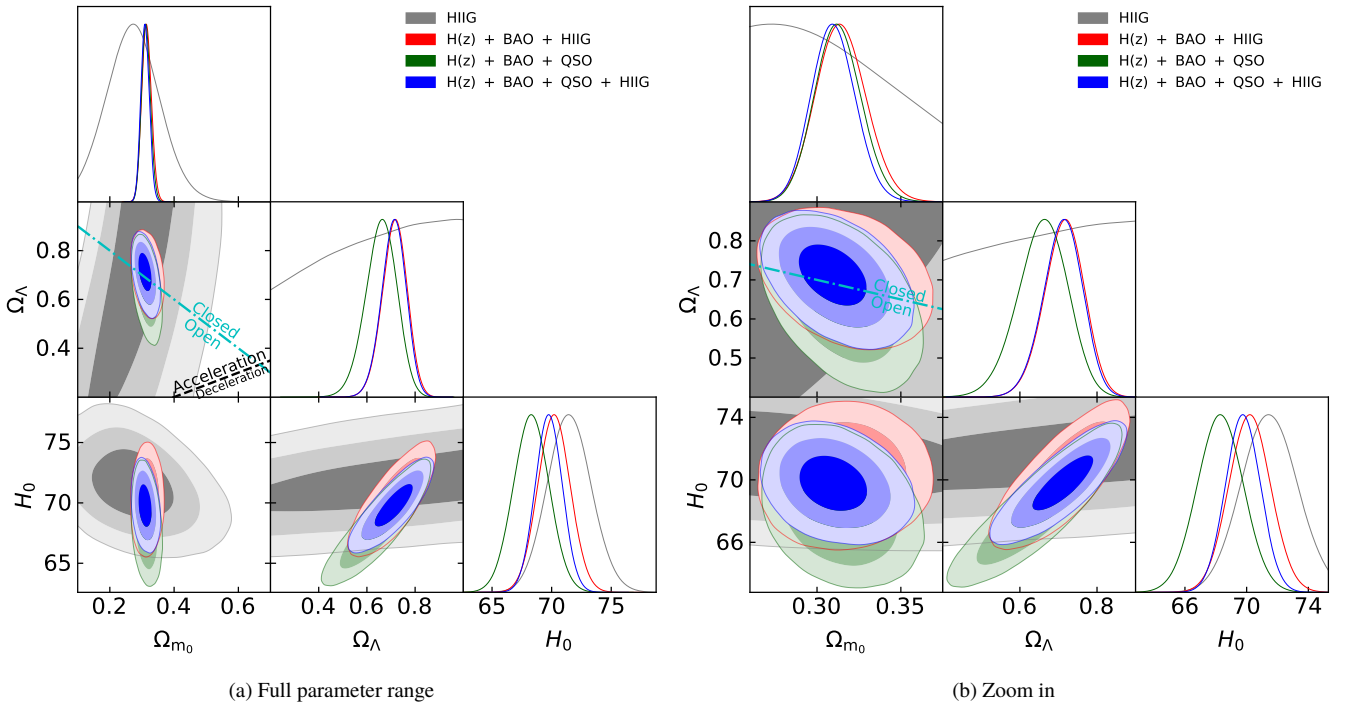


Figure 2. Same as Fig. 1 but for non-flat Λ CDM. The cyan dash-dot line represents the flat case, with closed spatial hypersurfaces to the upper right. The black dotted line is the zero-acceleration line, which divides the parameter space into regions associated with currently accelerated (above left) and currently decelerated (below right) cosmological expansion.

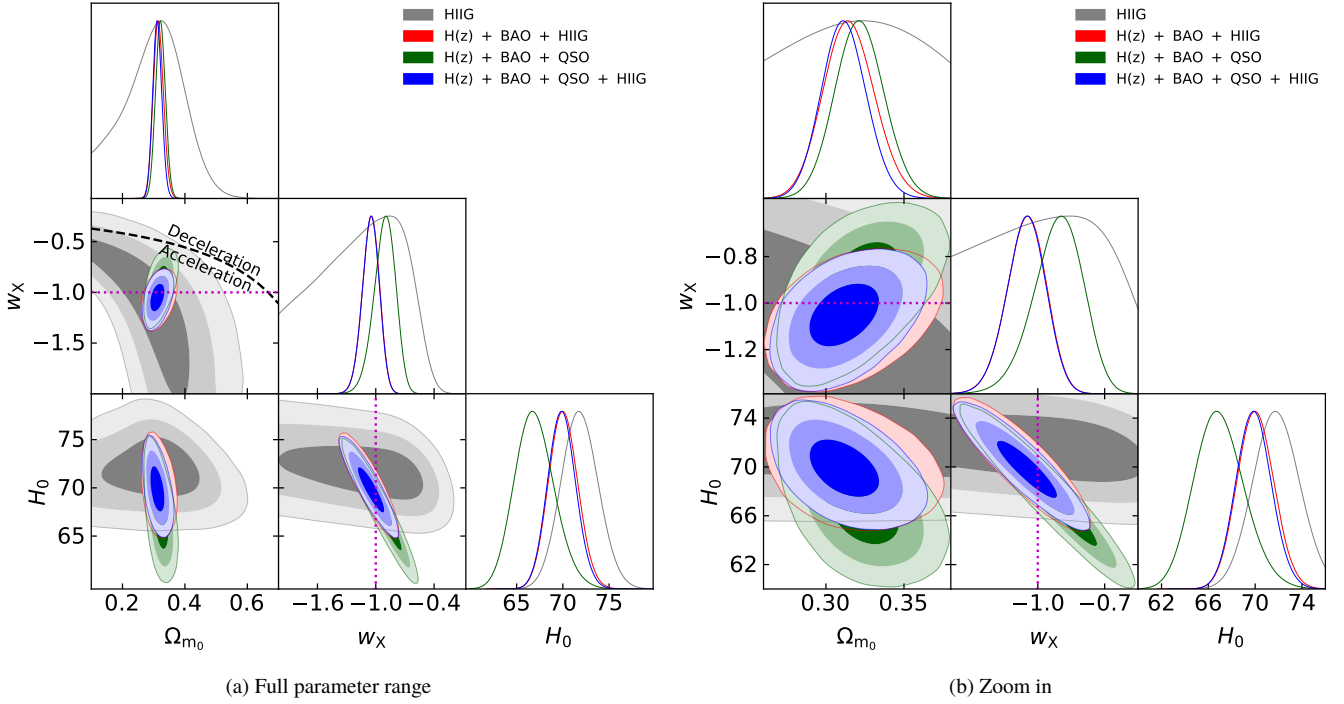


Figure 3. 1σ , 2σ , and 3σ confidence contours for flat XCDM. The black dotted line is the zero-acceleration line, which divides the parameter space into regions associated with currently accelerated (below left) and currently decelerated (above right) cosmological expansion. The magenta lines denote $w_X = -1$, i.e. the flat Λ CDM model.

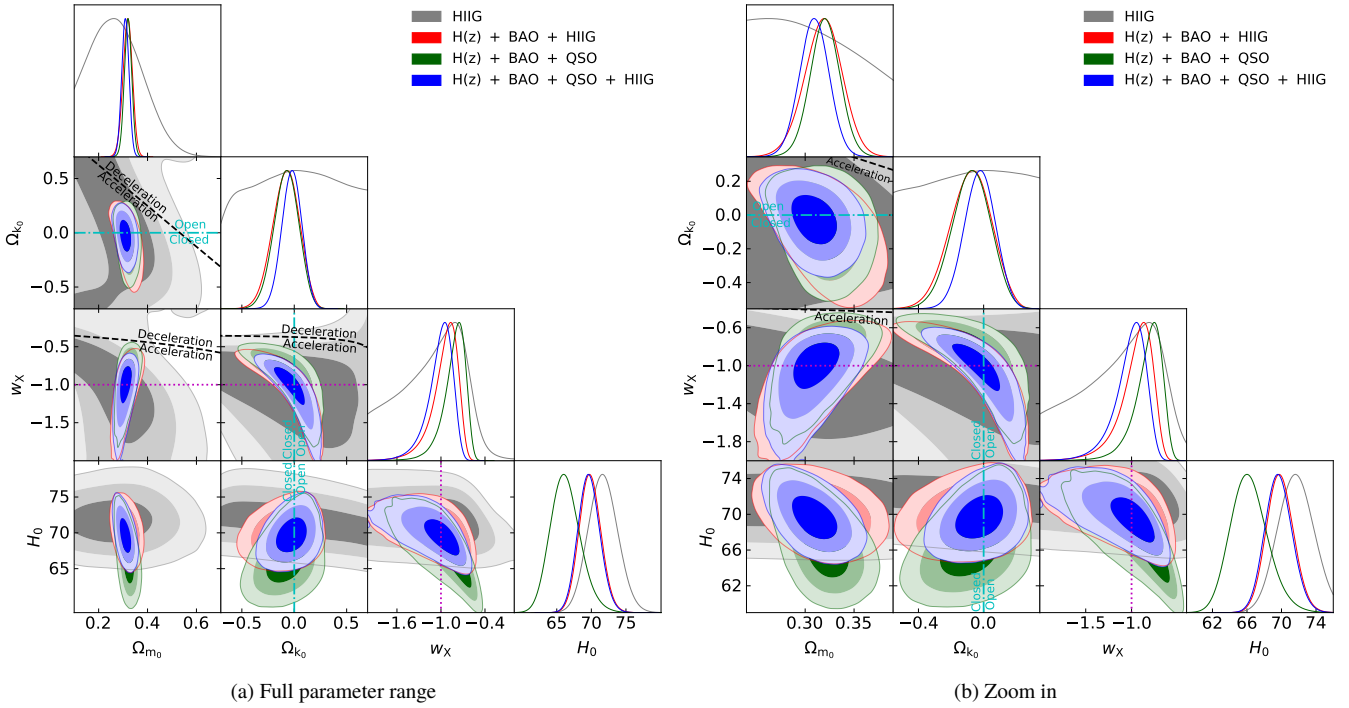


Figure 4. Same as Fig. 3 but for non-flat XCDM, where the zero acceleration lines in each of the three subpanels are computed for the third cosmological parameter set to the HIIG data only best-fit values listed in Table 2. Currently-accelerated cosmological expansion occurs below these lines. The cyan dash-dot lines represent the flat case, with closed spatial hypersurfaces either below or to the left. The magenta lines indicate $w_X = -1$, i.e. the non-flat Λ CDM model.

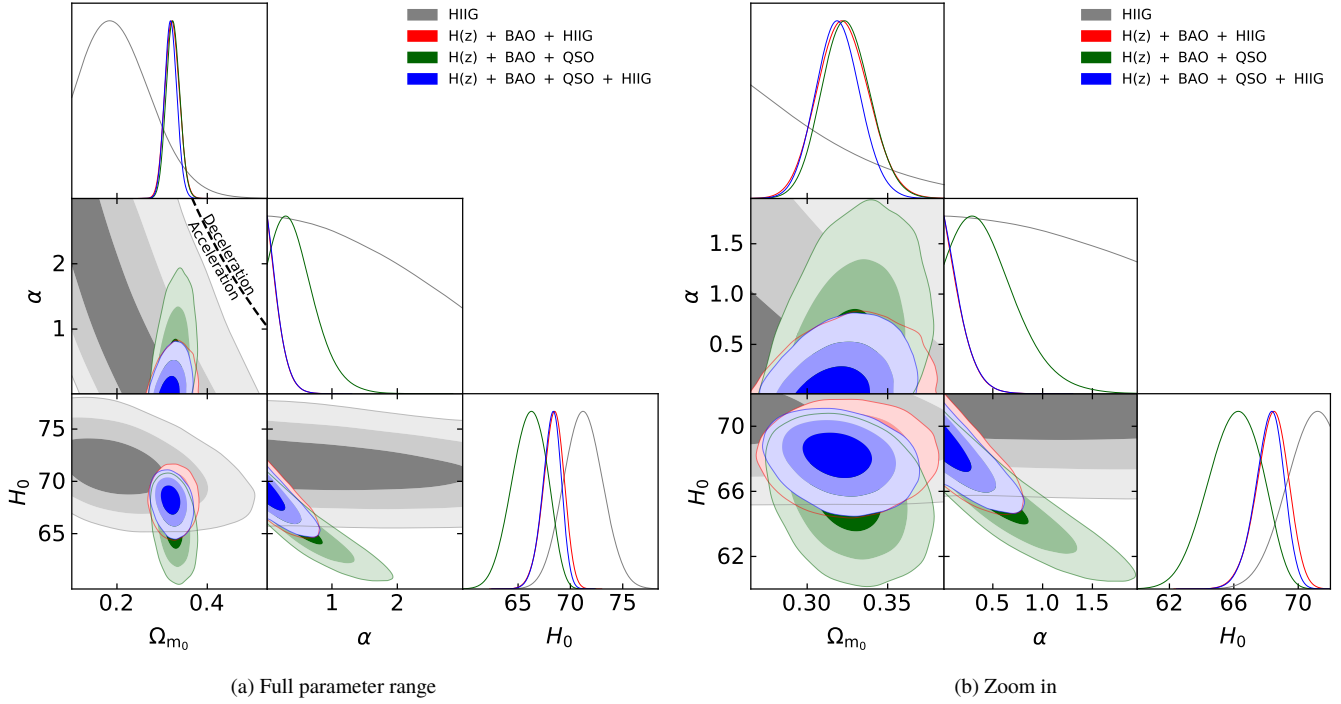


Figure 5. 1σ , 2σ , and 3σ confidence contours for flat ϕ CDM. The black dotted zero-acceleration line splits the parameter space into regions of currently accelerated (below left) and currently decelerated (above right) cosmological expansion. The $\alpha = 0$ axis is the flat Λ CDM model.

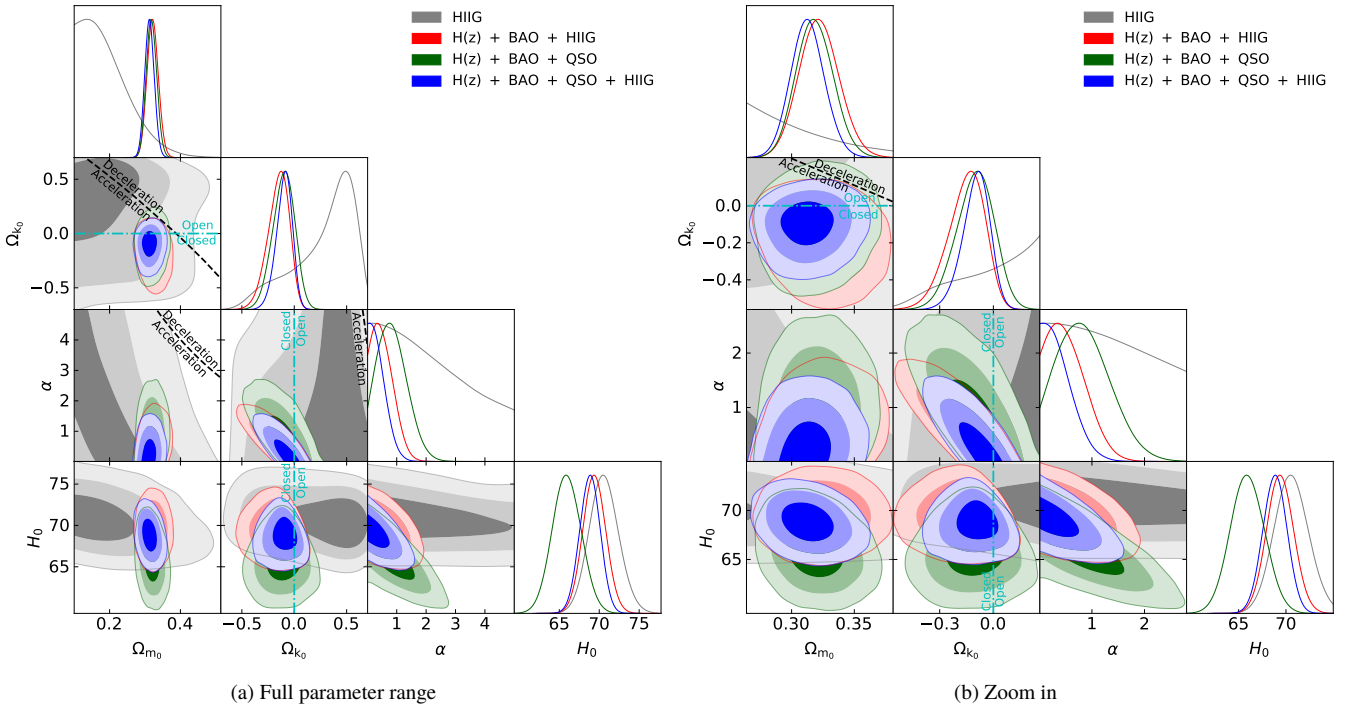


Figure 6. Same as Fig. 5 but for non-flat ϕ CDM, where the zero-acceleration lines in each of the subpanels are computed for the third cosmological parameter set to the HIIG data only best-fit values listed in Table 2. Currently-accelerating cosmological expansion occurs below these lines. The cyan dash-dot lines represent the flat case, with closed spatial geometry either below or to the left. The $\alpha = 0$ axis is the non-flat Λ CDM model.

2D confidence constraints for the HzBQH cases in blue. Tables 2 and 3 list the best-fit results and uncertainties.

It is interesting that the best-fit values of Ω_{m_0} in this case are lower compared with both the HzBQ and the HzBH results, being between $0.309^{+0.015}_{-0.014}$ (non-flat XCDM) and 0.319 ± 0.013 (flat ϕ CDM). The best-fit values of H_0 are higher than the HzBQ cases and have central values that are closer to those of the HzBH cases, but are still in better agreement with the lower median statistics estimate of H_0 (Chen & Ratra 2011a) than the higher local expansion rate measurement of H_0 (Riess et al. 2019), being between $68.18^{+0.97}_{-0.75}$ km s⁻¹ Mpc⁻¹ (flat ϕ CDM) and 69.90 ± 1.48 km s⁻¹ Mpc⁻¹ (flat XCDM).

For non-flat Λ CDM, non-flat XCDM, and non-flat ϕ CDM, we measure $\Omega_{k_0} = -0.021^{+0.044}_{-0.048}$, $\Omega_{k_0} = -0.025 \pm 0.092$, and $\Omega_{k_0} = -0.098^{+0.082}_{-0.061}$, respectively. For non-flat Λ CDM and XCDM, the measured values of the curvature energy density parameter are within 0.48σ and 0.27σ of $\Omega_{k_0} = 0$, respectively, while the non-flat ϕ CDM model favors a closed geometry with an Ω_{k_0} that is 1.20σ away from zero.

There is not much evidence in support of dark energy dynamics in the HzBQH case, with Λ consistent with this data combination. For flat (non-flat) XCDM, $w_X = -1.053^{+0.091}_{-0.082}$ ($w_X = -1.022^{+0.208}_{-0.104}$). For flat (non-flat) ϕ CDM, the 2σ upper limits are $\alpha < 0.411$ ($\alpha < 0.926$), which indicates that $\alpha = 0$ or Λ is consistent with these data.

5.5 Model comparison

From Table 4, we see that the reduced χ^2 for all models is relatively large (being between 2.25 and 2.75). This could probably be attributed to underestimated systematic uncertainties in the HIIG data.¹⁶ This is suggested by González-Morán et al. (2019), who also found relatively large values of χ^2/ν in their cosmological model fits to the HIIG data (though not as large as ours, because they compute a different χ^2 , as explained in footnote 10 in Sec. 4). They note that an additional systematic uncertainty of ~ 0.22 could bring their χ^2/ν down to ~ 1 . As mentioned previously, we do not account for HIIG systematic uncertainties in our analysis.

One thing that is clear, regardless of the absolute size of HIIG or QSO systematics (and ignoring the large values of χ^2/ν), is that the flat Λ CDM model remains the most favored model among the six models we studied, based on the AIC and BIC criteria (see Table 4).¹⁷ In Table 4 we define $\Delta\chi^2$, ΔAIC , and ΔBIC , respectively, as the differences between the values of the χ^2 , AIC , and BIC associated with a given model and their corresponding minimum values among all models.

From the HIIG results for ΔAIC and ΔBIC listed in Table 4, we see that the evidence against non-flat Λ CDM, flat XCDM, and flat ϕ CDM is weak (according to ΔAIC) and positive (according to ΔBIC) where, among these three models, the flat XCDM model is the least favored. The evidence against the non-flat XCDM model is weak regarding ΔAIC but strong based on ΔBIC , while the evidence against non-flat ϕ CDM in this case is positive (ΔAIC) and strong (ΔBIC), respectively, with it being the least favored model overall.

¹⁶ Underestimated systematic uncertainties might also explain the large reduced χ^2 of QSO data (Ryan et al. 2019).

¹⁷ Note that based on the $\Delta\chi^2$ results of Table 4 non-flat XCDM has the minimum χ^2 in the HIIG and HzBQ cases, whereas non-flat ϕ CDM has the minimum χ^2 for the HzBH and HzBQH cases. The $\Delta\chi^2$ values do not, however, penalize a model for having more parameters.

Largely similar conclusions result from ΔAIC and ΔBIC values for the HIIG and HzBQ data. The exception is that the HzBQ ΔAIC value gives only weak evidence against non-flat ϕ CDM, instead of the positive evidence against it from the HIIG ΔAIC value.

The HzBH and HzBQH values of ΔAIC and ΔBIC result in the following conclusions:

- 1) the evidence against both non-flat Λ CDM and flat XCDM is weak (HzBH) and positive (HzBQH) for ΔAIC and ΔBIC ;
- 2) the evidence against flat ϕ CDM is positive;
- 3) non-flat XCDM is the least favored model with non-flat ϕ CDM doing almost as badly. ΔAIC gives positive evidence against non-flat XCDM and non-flat ϕ CDM, while ΔBIC strongly disfavors (HzBH) and very strongly disfavors (HzBQH) both of these nonflat models.

6 CONCLUSION

In this paper, we have constrained cosmological parameters in six flat and non-flat cosmological models by analyzing a total of 315 observations, comprising 31 $H(z)$, 11 BAO, 120 QSO, and 153 HIIG measurements. The QSO angular size and HIIG apparent magnitude measurements are particularly noteworthy, as they reach to $z \sim 2.7$ and $z \sim 2.4$ respectively (somewhat beyond the highest $z \sim 2.3$ reached by BAO data) and into a much less studied area of redshift space. While the current HIIG and QSO data do not provide very restrictive constraints, they do tighten the limits when they are used in conjunction with BAO + $H(z)$ data.

By measuring cosmological parameters in a variety of cosmological models, we are able to draw some relatively model-independent conclusions (i.e. conclusions that do not differ significantly between the different models). Specifically, for the full data set (i.e. the HzBQH data), we find quite restrictive constraints on Ω_{m_0} , a reasonable summary perhaps being $\Omega_{m_0} = 0.310 \pm 0.013$, in good agreement with many other recent estimates. H_0 is also fairly tightly constrained, with a reasonable summary perhaps being $H_0 = 69.5 \pm 1.2$ km s⁻¹ Mpc⁻¹, which is in better agreement with the results of Chen & Ratra (2011a) and Planck Collaboration (2018) than that of Riess et al. (2019). The HzBQH measurements are consistent with the standard spatially-flat Λ CDM model, but do not strongly rule out mild dark energy dynamics or a little spatial curvature energy density. More and better-quality HIIG, QSO, and other data at $z \sim 2-4$ will significantly help to test these extensions.

ACKNOWLEDGEMENTS

We thank Ana Luisa González-Morán and Ricardo Chávez for useful information and discussions related to the HIIG data, and Javier de Cruz Pérez and Chan-Gyung Park for useful discussions on the BAO data. Additionally, we thank Adam Riess for his comments on an early version of this paper, and the anonymous referee for useful suggestions. This work was partially funded by Department of Energy grants DE-SC0019038 and DE-SC0011840. Some of the computing for this project was performed on the Beocat Research Cluster at Kansas State University, which is funded in part by NSF grants CNS-1006860, EPS-1006860, EPS-0919443, ACI-1440548, CHE-1726332, and NIH P20GM113109.

Table 4. $\Delta\chi^2$, ΔAIC , ΔBIC , and χ^2_{\min}/ν values.

Quantity	Data set	Flat Λ CDM	Non-flat Λ CDM	Flat XCDM	Non-flat XCDM	Flat ϕ CDM	Non-flat ϕ CDM
$\Delta\chi^2$	HIIG	3.06	2.75	3.03	0.00	3.01	2.22
	$H(z)$ + BAO + HIIG	1.54	0.63	1.24	0.10	1.61	0.00
	$H(z)$ + BAO + QSO	2.20	2.14	1.27	0.00	1.37	0.15
	$H(z)$ + BAO + QSO + HIIG	0.85	0.14	0.54	0.05	0.93	0.00
ΔAIC	HIIG	0.00	1.69	1.97	0.94	1.95	3.16
	$H(z)$ + BAO + HIIG	0.00	1.09	1.70	2.56	2.07	2.46
	$H(z)$ + BAO + QSO	0.00	1.94	1.07	1.80	1.17	1.95
	$H(z)$ + BAO + QSO + HIIG	0.00	1.29	1.69	3.20	2.08	3.15
ΔBIC	HIIG	0.00	4.72	5.01	7.00	4.99	9.22
	$H(z)$ + BAO + HIIG	0.00	4.35	4.97	9.10	5.34	9.00
	$H(z)$ + BAO + QSO	0.00	5.02	4.15	7.97	4.25	8.12
	$H(z)$ + BAO + QSO + HIIG	0.00	5.04	5.44	10.70	5.83	10.65
χ^2_{\min}/ν	HIIG	2.72	2.74	2.74	2.74	2.74	2.75
	$H(z)$ + BAO + HIIG	2.25	2.26	2.26	2.27	2.26	2.27
	$H(z)$ + BAO + QSO	2.33	2.34	2.34	2.35	2.34	2.35
	$H(z)$ + BAO + QSO + HIIG	2.51	2.52	2.52	2.53	2.52	2.53

DATA AVAILABILITY

The HIIG data underlying this article were provided to us by the authors of [González-Morán et al. \(2019\)](#). These data will be shared on request to the corresponding author with the permission of the authors of [González-Morán et al. \(2019\)](#).

REFERENCES

- Alam S., et al., 2017, *MNRAS*, **470**, 2617
- Ata M., et al., 2018, *MNRAS*, **473**, 4773
- Aubourg É., et al., 2015, *Phys. Rev. D*, **92**, 123516
- Avsajanishvili O., Samushia L., Arhipova N. A., Kahniashvili T., 2015, preprint, ([arXiv:1511.09317](#))
- Campanelli L., Fogli G. L., Kahniashvili T., Marrone A., Ratra B., 2012, *European Physical Journal C*, **72**, 2218
- Cao S., Zheng X., Biesiada M., Qi J., Chen Y., Zhu Z.-H., 2017, *A&A*, **606**, A15
- Carter P., Beutler F., Percival W. J., Blake C., Koda J., Ross A. J., 2018, *MNRAS*, **481**, 2371
- Chávez R., Terlevich E., Terlevich R., Plionis M., Bresolin F., Basilakos S., Melnick J., 2012, *MNRAS*, **425**, L56
- Chávez R., Terlevich R., Terlevich E., Bresolin F., Melnick J., Plionis M., Basilakos S., 2014, *MNRAS*, **442**, 3565
- Chávez R., Plionis M., Basilakos S., Terlevich R., Terlevich E., Melnick J., Bresolin F., González-Morán A. L., 2016, *MNRAS*, **462**, 2431
- Chen G., Ratra B., 2003, *ApJ*, **582**, 586
- Chen G., Ratra B., 2004, *ApJ*, **612**, L1
- Chen G., Ratra B., 2011a, *PASP*, **123**, 1127
- Chen Y., Ratra B., 2011b, *Physics Letters B*, **703**, 406
- Chen G., Gott III J. R., Ratra B., 2003, *PASP*, **115**, 1269
- Chen Y., Ratra B., Biesiada M., Li S., Zhu Z.-H., 2016, *ApJ*, **829**, 61
- Chen Y., Kumar S., Ratra B., 2017, *ApJ*, **835**, 86
- Coley A. A., 2019, preprint, ([arXiv:1905.04588](#))
- Coley A. A., Ellis G. F. R., 2020, *Classical and Quantum Gravity*, **37**, 013001
- Cuceu A., Farr J., Lemos P., Font-Ribera A., 2019, *J. Cosmology Astropart. Phys.*, **2019**, 044
- DES Collaboration 2018, *MNRAS*, **480**, 3879
- DES Collaboration 2019a, *Phys. Rev. D*, **99**, 123505
- DES Collaboration 2019b, *MNRAS*, **483**, 4866
- de Sainte Agathe V., et al., 2019, *A&A*, **629**, A85
- Demianski M., Piedipalumbo E., Sawant D., Amati L., 2019, preprint, ([arXiv:1911.08228](#))
- Dhawan S., Jha S. W., Leibundgut B., 2018, *A&A*, **609**, A72
- Di Valentino E., Melchiorri A., Silk J., 2020, preprint, ([arXiv:2003.04935](#))
- Domínguez A., et al., 2019, *ApJ*, **885**, 137
- Efstathiou G., Grattón S., 2020, preprint, ([arXiv:2002.06892](#))
- Erb D. K., Steidel C. C., Shapley A. E., Pettini M., Reddy N. A., Adelberger K. L., 2006, *ApJ*, **646**, 107
- Farooq O., Ratra B., 2013, *ApJ*, **766**, L7
- Farooq O., Crandall S., Ratra B., 2013, *Physics Letters B*, **726**, 72
- Farooq O., Mania D., Ratra B., 2015, *Ap&SS*, **357**, 11
- Farooq O., Ranjeet Madiyar F., Crandall S., Ratra B., 2017, *ApJ*, **835**, 26
- Fernández Arenas D., et al., 2018, *MNRAS*, **474**, 1250
- Foreman-Mackey D., Hogg D. W., Lang D., Goodman J., 2013, *PASP*, **125**, 306
- Freedman W. L., et al., 2019, *ApJ*, **882**, 34
- Freedman W. L., et al., 2020, *ApJ*, **891**, 57
- Gao C., Chen Y., Zheng J., 2020, preprint, ([arXiv:2004.09291](#))
- Geng C.-Q., Hsu Y.-T., Yin L., Zhang K., 2020, preprint, ([arXiv:2002.05290](#))
- Gómez-Valent A., Amendola L., 2018, *J. Cosmology Astropart. Phys.*, **4**, 051
- González-Morán A. L., et al., 2019, *MNRAS*, **487**, 4669
- Gordon K. D., Clayton G. C., Misselt K. A., Landolt A. U., Wolff M. J., 2003, *ApJ*, **594**, 279
- Gott III J. R., Vogeley M. S., Podariu S., Ratra B., 2001, *ApJ*, **549**, 1
- Gurvits L. I., Kellermann K. I., Frey S., 1999, *A&A*, **342**, 378
- Handley W., 2019, *Phys. Rev. D*, **100**, 123517
- Haridasu B. S., Luković V. V., Moresco M., Vittorio N., 2018, *J. Cosmology Astropart. Phys.*, **2018**, 015
- Hogg D. W., 1999, preprint, ([arXiv:astro-ph/9905116](#))
- Jesus J. F., Valentim R., Moraes P. H. R. S., Malheiro M., 2019, preprint, ([arXiv:1907.01033](#))
- Khadka N., Ratra B., 2020a, preprint, ([arXiv:2004.09979](#))
- Khadka N., Ratra B., 2020b, *MNRAS*, **492**, 4456
- Kumar D., Jain D., Mahajan S., Mukherjee A., Rani N., 2020, preprint, ([arXiv:2002.06354](#))
- Lamb D. Q., Reichart D. E., 2000, *ApJ*, **536**, 1
- Lewis A., 2019, preprint, ([arXiv:1910.13970](#))
- Li E.-K., Du M., Xu L., 2020, *MNRAS*, **491**, 4960
- Lin W., Ishak M., 2019, preprint, ([arXiv:1909.10991](#))
- Mania D., Ratra B., 2012, *Physics Letters B*, **715**, 9
- Martin J., 2012, *Comptes Rendus Physique*, **13**, 566
- Martinelli M., Tutusaus I., 2019, preprint, ([arXiv:1906.09189](#))
- Maseda M. V., et al., 2014, *ApJ*, **791**, 17
- Masters D., et al., 2014, *ApJ*, **785**, 153
- Melnick J., Terlevich R., Terlevich E., 2000, *MNRAS*, **311**, 629
- Melnick J., et al., 2017, *A&A*, **599**, A76
- Moresco M., Jimenez R., Verde L., Pozzetti L., Cimatti A., Citro A., 2018, *ApJ*, **868**, 84

- Moresco M., Jimenez R., Verde L., Cimatti A., Pozzetti L., 2020, arXiv e-prints, p. [arXiv:2003.07362](https://arxiv.org/abs/2003.07362)
- Ooba J., Ratra B., Sugiyama N., 2018a, *ApJ*, **864**, 80
- Ooba J., Ratra B., Sugiyama N., 2018b, *ApJ*, **866**, 68
- Ooba J., Ratra B., Sugiyama N., 2018c, *ApJ*, **869**, 34
- Ooba J., Ratra B., Sugiyama N., 2019, *Ap&SS*, **364**, 176
- Park C.-G., Ratra B., 2018, *ApJ*, **868**, 83
- Park C.-G., Ratra B., 2019a, *Ap&SS*, **364**, 82
- Park C.-G., Ratra B., 2019b, *Ap&SS*, **364**, 134
- Park C.-G., Ratra B., 2019c, *ApJ*, **882**, 158
- Park C.-G., Ratra B., 2020, *Phys. Rev. D*, **101**, 083508
- Pavlov A., Westmoreland S., Saaïdi K., Ratra B., 2013, *Phys. Rev. D*, **88**, 123513
- Peebles P. J. E., 1984, *ApJ*, **284**, 439
- Peebles P. J. E., Ratra B., 1988, *ApJ*, **325**, L17
- Planck Collaboration 2018, preprint, ([arXiv:1807.06209](https://arxiv.org/abs/1807.06209))
- Plionis M., Terlevich R., Basilakos S., Bresolin F., Terlevich E., Melnick J., Georgantopoulos I., 2009, in *Journal of Physics Conference Series*. p. 012032 ([arXiv:0903.0131](https://arxiv.org/abs/0903.0131))
- Plionis M., Terlevich R., Basilakos S., Bresolin F., Terlevich E., Melnick J., Chavez R., 2010, in Alimi J.-M., Fuözfa A., eds, *American Institute of Physics Conference Series* Vol. 1241, American Institute of Physics Conference Series. pp 267–276 ([arXiv:0911.3198](https://arxiv.org/abs/0911.3198))
- Plionis M., Terlevich R., Basilakos S., Bresolin F., Terlevich E., Melnick J., Chavez R., 2011, *MNRAS*, **416**, 2981
- Rameez M., Sarkar S., 2019, preprint, ([arXiv:1911.06456](https://arxiv.org/abs/1911.06456))
- Rana A., Jain D., Mahajan S., Mukherjee A., 2017, *J. Cosmology Astropart. Phys.*, **3**, 028
- Ratra B., Peebles P. J. E., 1988, *Phys. Rev. D*, **37**, 3406
- Ratra B., Vogeley M. S., 2008, *PASP*, **120**, 235
- Riess A. G., 2019, *Nature Reviews Physics*, **2**, 10
- Riess A. G., Casertano S., Yuan W., Macri L. M., Scolnic D., 2019, *ApJ*, **876**, 85
- Rigault M., et al., 2015, *ApJ*, **802**, 20
- Risaliti G., Lusso E., 2015, *ApJ*, **815**, 33
- Risaliti G., Lusso E., 2019, *Nature Astronomy*, **3**, 272
- Ruan C.-Z., Melia F., Chen Y., Zhang T.-J., 2019, *ApJ*, **881**, 137
- Ryan J., Doshi S., Ratra B., 2018, *MNRAS*, **480**, 759
- Ryan J., Chen Y., Ratra B., 2019, *MNRAS*, **488**, 3844
- Samushia L., Ratra B., 2010, *ApJ*, **714**, 1347
- Samushia L., Chen G., Ratra B., 2007, preprint, ([arXiv:0706.1963](https://arxiv.org/abs/0706.1963))
- Samushia L., Dev A., Jain D., Ratra B., 2010, *Physics Letters B*, **693**, 509
- Sangwan A., Tripathi A., Jassal H. K., 2018, preprint, ([arXiv:1804.09350](https://arxiv.org/abs/1804.09350))
- Schöneberg N., Lesgourgues J., Hooper D. C., 2019, *J. Cosmology Astropart. Phys.*, **2019**, 029
- Scolnic D. M., et al., 2018, *ApJ*, **859**, 101
- Siegel E. R., Guzmán R., Gallego J. P., Orduña López M., Rodríguez Hidalgo P., 2005, *MNRAS*, **356**, 1117
- Singh A., Sangwan A., Jassal H. K., 2019, *J. Cosmology Astropart. Phys.*, **2019**, 047
- Solà Peracaula J., de Cruz Pérez J., Gómez-Valent A., 2018, *MNRAS*, **478**, 4357
- Solà Peracaula J., Gómez-Valent A., de Cruz Pérez J., 2019, *Physics of the Dark Universe*, **25**, 100311
- Solà J., Gómez-Valent A., de Cruz Pérez J., 2017, *Modern Physics Letters A*, **32**, 1750054
- Terlevich R., Terlevich E., Melnick J., Chávez R., Plionis M., Bresolin F., Basilakos S., 2015, *MNRAS*, **451**, 3001
- Wan H.-Y., Cao S.-L., Melia F., Zhang T.-J., 2019, *Physics of the Dark Universe*, **26**, 100405
- Wang B., Qi J.-Z., Zhang J.-F., Zhang X., 2019, preprint, ([arXiv:1910.12173](https://arxiv.org/abs/1910.12173))
- Wei J.-J., 2018, *ApJ*, **868**, 29
- Wei J.-J., Wu X.-F., Melia F., 2016, *MNRAS*, **463**, 1144
- Wu Y., Cao S., Zhang J., Liu T., Liu Y., Geng S., Lian Y., 2020, *ApJ*, **888**, 113
- Yang T., Banerjee A., Colgáin E. Ó., 2019, preprint, p. [arXiv:1911.01681](https://arxiv.org/abs/1911.01681) ([arXiv:1911.01681](https://arxiv.org/abs/1911.01681))
- Yashar M., Bozek B., Abrahamse A., Albrecht A., Barnard M., 2009, *Phys. Rev. D*, **79**, 103004
- Yennapureddy M. K., Melia F., 2017, *J. Cosmology Astropart. Phys.*, **2017**, 029
- Yu H., Wang F. Y., 2016, *ApJ*, **828**, 85
- Yu H., Ratra B., Wang F.-Y., 2018, *ApJ*, **856**, 3
- Zeng H., Yan D., 2019, *ApJ*, **882**, 87
- Zhai Z., Blanton M., Slosar A., Tinker J., 2017, *ApJ*, **850**, 183
- Zhai Z., Park C.-G., Wang Y., Ratra B., 2019, preprint, ([arXiv:1912.04921](https://arxiv.org/abs/1912.04921))
- Zhang J., 2018, *PASP*, **130**, 084502
- Zhang X., Huang Q.-G., 2019, preprint, ([arXiv:1911.09439](https://arxiv.org/abs/1911.09439))
- Zhang B. R., Childress M. J., Davis T. M., Karpenka N. V., Lidman C., Schmidt B. P., Smith M., 2017, *MNRAS*, **471**, 2254
- Zheng J., Melia F., Zhang T.-J., 2019, preprint, ([arXiv:1901.05705](https://arxiv.org/abs/1901.05705))
- Zheng X., Liao K., Biesiada M., Cao S., Liu T.-H., Zhu Z.-H., 2020, *ApJ*, **892**, 103

This paper has been typeset from a $\text{\TeX}/\text{\LaTeX}$ file prepared by the author.